



This is a repository copy of *Influence of stator topologies on average torque and torque ripple of fractional-slot SPM machines with fully closed slots.*

White Rose Research Online URL for this paper:
<http://eprints.whiterose.ac.uk/126079/>

Version: Accepted Version

Article:

Li, Y.X., Zhu, Z.Q. and Li, G. (2018) Influence of stator topologies on average torque and torque ripple of fractional-slot SPM machines with fully closed slots. *IEEE Transactions on Industry Applications*, 54 (3). pp. 2151-2164. ISSN 0093-9994

<https://doi.org/10.1109/TIA.2018.2799178>

© 2018 IEEE. Personal use of this material is permitted. Permission from IEEE must be obtained for all other users, including reprinting/ republishing this material for advertising or promotional purposes, creating new collective works for resale or redistribution to servers or lists, or reuse of any copyrighted components of this work in other works. Reproduced in accordance with the publisher's self-archiving policy.

Reuse

Items deposited in White Rose Research Online are protected by copyright, with all rights reserved unless indicated otherwise. They may be downloaded and/or printed for private study, or other acts as permitted by national copyright laws. The publisher or other rights holders may allow further reproduction and re-use of the full text version. This is indicated by the licence information on the White Rose Research Online record for the item.

Takedown

If you consider content in White Rose Research Online to be in breach of UK law, please notify us by emailing eprints@whiterose.ac.uk including the URL of the record and the reason for the withdrawal request.



eprints@whiterose.ac.uk
<https://eprints.whiterose.ac.uk/>

Influence of Stator Topologies on Average Torque and Torque Ripple of Fractional-Slot SPM Machines with Fully Closed Slots

Y. X. Li, Z. Q. Zhu, Fellow, IEEE, and G. J. Li, Senior Member, IEEE

Abstract—This paper investigates the influence of concentrated winding configurations and stator core structures on torque performance of fractional-slot surface-mounted PM (SPM) machines. From analyzing the separated torque components of prototype SPM machines with 12-slots/10-poles (12S/10P) combination by frozen permeability (FP) method, it can be found that the torque ripple is closely related with local saturation in fully closed slot (FCS) machines. Besides, the heavier local saturation will also jeopardize the merit of using alternate teeth wound windings, such as obtaining higher average torque than electrical machines with all teeth wound windings. The further analysis of stator tooth relative permeability variation over one electrical period demonstrates that the major reason for torque ripple difference among these electrical machines with different stator topologies is the asymmetric saturation between the adjacent teeth. Both the subharmonic due to armature reaction (determined by winding connection and current value) and the asymmetry of stator core structure contribute to such asymmetric saturation. In order to more clearly verify this, the complementary slot/pole number combination (12S/14P) is also analyzed. The conclusion is effective for electrical machines with other slot/pole number combinations as well. Experiments have been carried out to validate the predictions.

Index Terms— Asymmetric saturation, average torque, local saturation, stator core structure, torque ripple, winding configuration.

I. INTRODUCTION

Fractional-slot PM machines with non-overlapping windings have been widely investigated and applied over the past few decades due to the merits of high torque density, low torque ripple and high efficiency, etc. [1].

The basic theory of fractional-slot PM machines with non-overlapping windings has been introduced in detail [2], especially the conditions for constructing such kind of windings. The authors from [3] employed and extended the star of slot method to fractional-slot machines. Based on the proposed method, the slot/pole number combinations for all and alternate teeth wound windings (abbreviated as “All” and “Alternate” in the figures for simplicity throughout this paper) were summarized in [3]. The comparison between the electrical machines with all and alternate teeth wound windings were performed in [4] which addressed one advantage of the alternate teeth wound winding, viz. better fault-tolerant capability. The further comparison between these two kinds of

windings in terms of torque-speed characteristic was shown in [5]. The parasitic effects of adopting non-overlapping windings were analyzed in [6], especially the radial force density differences between different winding topologies. Another merit that the flux-weakening capability can be increased by adopting alternate teeth wound winding was highlighted in [7]. The more comprehensive study of all and alternate teeth wound windings can be seen in [8]-[9]. In order to increase the average torque, both all and alternate teeth wound windings can fulfil this by some modifications. For machines with all teeth wound winding, dual 3-phase winding (abbreviated as “D3p”) configuration with 30 electrical degree phase shift between two sets of windings can be adopted compared with the conventional single 3-phase winding (abbreviated as “S3p”). This not only increases the output torque but decreases torque ripple as well. The corresponding slot/pole number combinations for this kind of winding connection was summarized in [10]. The comparison between single and dual 3-phase windings was shown in [11] by analyzing 12-slots/10-poles (12S/10P) PM machines. On the other hand, the electrical machines with alternate teeth wound windings will obtain a higher average torque by using unequal tooth width (abbreviated as “UETW”) stator core structure. Although this idea was mentioned in [1], the reason for improving the average torque by adopting this kind of structure was elaborated in [12]. More comments about this stator core structure were given in [13].

However, both the average torque and the torque ripple should be considered in high precision application cases, such as servo control. From this point of view, adopting alternate teeth wound winding is worse than all teeth wound one [8]. Furthermore, UETW stator could lead to a higher torque ripple though it may generate higher average torque compared with equal tooth width (abbreviated as “ETW”) stator [12]. Only adjusting the all teeth wound winding connection from single 3-phase to dual 3-phase can effectively reduce torque ripple [11], whereas another set of inverter is needed. Therefore, both the average torque and torque ripple need to be investigated together. According to the analysis in [14]-[15], the reason for higher torque ripple in electrical machines with alternate teeth wound windings was the higher saturation caused by subharmonic. The torque separation with the help of frozen permeability (FP) method was shown in [16]-[17]. However, they concerned more on average torque. Although the authors

from [18] analyzed both aspects, only single 3-phase all teeth wound winding was shown. The influence of saturation caused by subharmonic was also stressed in [19], whereas only vibration was emphasized. Most of the above papers focused on machines with slot openings and quite a few researchers have investigated the influence of slot opening on torque performances [20]-[22]. Although the open-circuit cogging torque is almost eliminated by adopting fully closed slot (abbreviated as “FCS”) stator [20], the on-load average torque will reduce as well [21]. Besides, the on-load terminal voltage will be distorted due to local saturation [22]. However, these papers just analyzed one specific electrical machine and the influence of stator topologies on torque performance for FCS machines has not been shown before.

This paper extends the analysis in [23]. For a clear explanation, only surface-mounted PM (SPM) electrical machines having 12S/10P combination are chosen as example. The on-load torque of prototype machines with different concentrated winding topologies and stator core structures are shown and compared firstly. The influence of local saturation due to FCSs is also addressed. Then, the FP method is employed to separate the on-load torque into PM, armature and cogging torque components for detailed analysis. The reason for torque ripple difference between these electrical machines is addressed as well, together with the analysis of current value influence on torque performance. Moreover, the results of electrical machines with the complementary slot/pole number combination (12S/14P) are also shown to further verify the conclusion. Finally, some experimental results are presented to validate the correctness of the analysis.

II. MACHINE TOPOLOGIES UNDER INVESTIGATION

The cross-sections of 12S/10P prototype machines analyzed in the paper are shown in Fig. 1, together with the winding layouts. For simplicity, they are named by the abbreviation form which shows the winding arrangement, stator core structure and current supply pattern, viz. All ETW S3p, All ETW D3p, Alternate ETW S3p and Alternate UETW S3p machine, respectively. In order to make the comparison as reasonable as possible, all of the machines have been optimized with the same rotor, stator inner/outer diameter, total coil turns and peak current value. As can also be seen in Fig. 1, the FCSs are adopted, which will ideally eliminate the open-circuit cogging torque. Some different phenomena are expected to be observed in these machines compared with those having slot openings. It is worth noting that two sets of windings have 30 electrical degree phase shift between each other for the All ETW D3p machine. The stator yoke thickness of the Alternate UETW S3p machine was increased in accordance with the thick teeth to ensure the machine not oversaturated. The major parameters of these PM machines are listed in TABLE I.

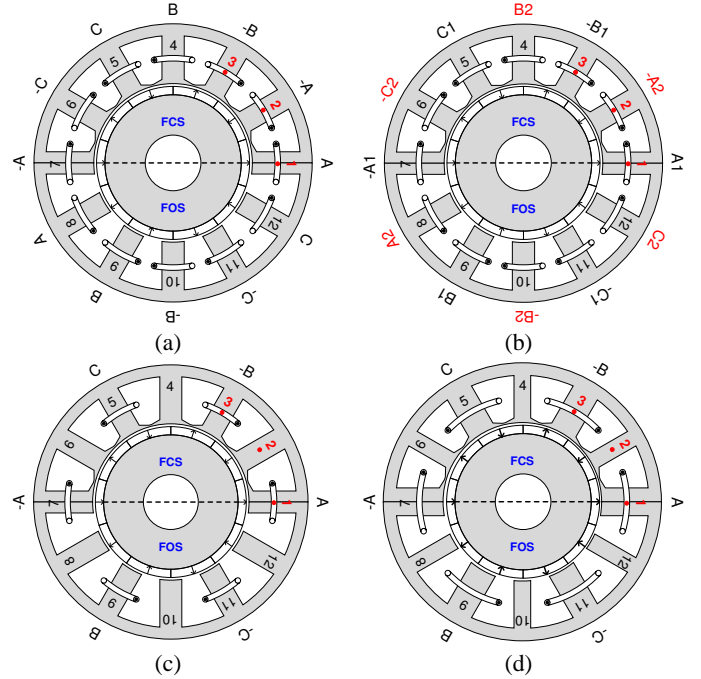


Fig. 1. Cross-sections of prototype PM machines with 12S/10P combination. (a) All ETW S. (b) All ETW D3p. (c) Alternate ETW S3p. (d) Alternate UETW S3p.

TABLE I MAJOR PARAMETERS OF PROTOTYPE MACHINES

Item	All ETW S3p	All ETW D3p	Alternate ETW S3p	Alternate UETW S3p
Stator outer diameter (mm)			100	
Stator inner diameter (mm)			57	
Stator yoke thickness (mm)	4	4	4	5
Stator tooth width (mm)	8	8	8	10 ^a and 6 ^b
Tooth bridge thickness for FCS (mm)			0.6	
Slot opening for FOS (mm)			6.9	
Air-gap length (mm)			1	
PM thickness (mm)			3	
PM remanence (T)			1.2	
PM relative permeability			1.05	
Turns per phase	184	92	184	184
Peak rated current (A)			10	
Rated speed (rpm)			400	

^a the tooth with a coil,

^b the tooth without a coil.

III. COMPARATIVE STUDY OF TORQUE

A. Comparison of On-load Torque

Since all of the electrical machines are surface-mounted type, the difference between d- and q-axis is pretty small, viz. negligible reluctance torque [1]. Therefore, zero d-axis current control strategy is adopted. When all of them are supplied with rated current, the corresponding torque is shown in Fig. 2 and the major information about torque performances are summarized in TABLE II. Since the FCS machines have strong local saturation compared with the fully open slot (abbreviated as “FOS”) counterparts shown in Fig.1, the on-load torque of FOS machines are also given to illustrate this effect. The winding factors of working harmonic (k_w), viz. rotor pole pair number, predicted by the methods in [3] and [12] are given to show the inherent property of each kind of winding. It consists

of winding pitch factor (k_p) and distribution factor (k_d). For prototype machines, the calculation methods are summarized in TABLE III, where p , N_s and m represent the rotor pole pair number, stator tooth number and phase number, respectively. There is also one parameter called ‘Ratio’ being defined as the ratio of average torque to the winding factor in TABLE II. This parameter can be used to evaluate the electrical machine saturation level. The reason can be explained based on the simplified average torque prediction equation.

$$T_{avg} = \frac{m}{2} p \psi_d I_q = \frac{\pi D_{gap}}{4} m N_{ph} l_{ef} k_w B_{gravg} I_q \propto k_w B_{gravg} I_q \quad (1)$$

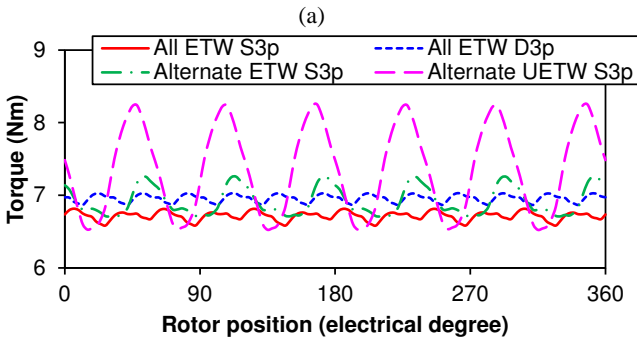
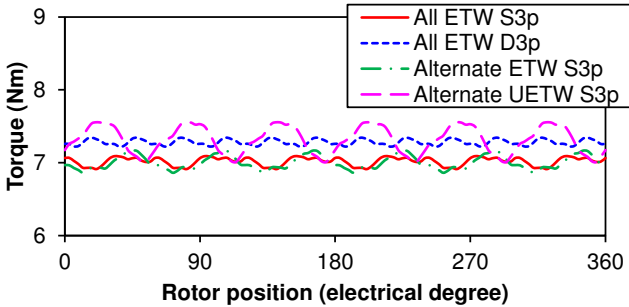
$$\text{Ratio} = \frac{T_{avg}}{k_w} = \frac{\pi D_{gap}}{4} m N_{ph} l_{ef} B_{gravg} I_q \propto B_{gravg} I_q$$

where ψ_d is the d-axis flux-linkage accounting for q-axis current (I_q) influence; D_{gap} is the air-gap center diameter; N_{ph} is the turns per phase; l_{ef} is the electrical machine axial effective length and B_{gravg} is the average radial air-gap flux density over one pole pitch.

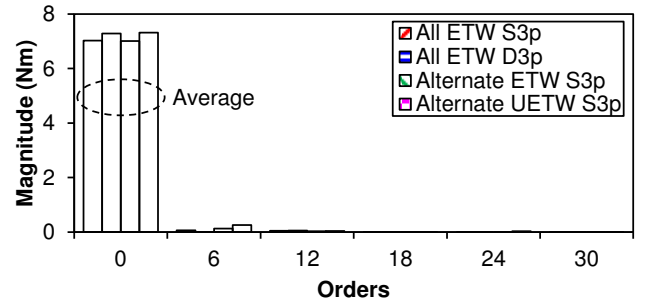
According to (1), the average torques of four prototype machines are mainly determined by k_w , B_{gravg} and I_q due to the constraints listed in TABLE I. Among three parameters, k_w is determined by winding intrinsic property and the product of B_{gravg} and I_q can reflect electrical machine saturation level caused by armature winding current for the same rotor PM excitation. Therefore, the influence of k_w should be eliminated. That is why the parameter ‘Ratio’ is defined, as stated above. For torque ripple, it is calculated by:

$$\text{Torque Ripple} = \frac{T_{pp}}{T_{avg}} \times 100\% \quad (2)$$

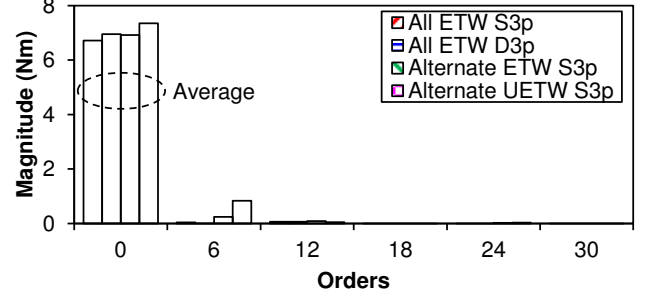
where T_{pp} is the peak to peak torque ripple and T_{avg} is the average torque over one electrical period.



(b)



(c)



(d)

Fig. 2. On-load torque comparison (Rated). (a) Waveforms for FCS machines. (b) Waveforms for FOS machines. (c) Spectra for FCS machines. (d) Spectra for FOS machines.

TABLE II CHARACTERISTIC VALUES FOR TORQUE COMPARISON OF 12S/10P COMBINATION

Machine type	Average torque (Nm)	Winding factor	Ratio	PP torque ripple (Nm)	Torque ripple (%)
All ETW S3p FCS	7.02	0.9330	7.52	0.18	2.53
All ETW S3p FOS	6.71		7.19	0.23	3.48
All ETW D3p FCS	7.28	0.9659	7.54	0.12	1.65
All ETW D3p FOS	6.96		7.21	0.16	2.30
Alternate ETW S3p FCS	7.00	0.9659	7.22	0.34	4.35
Alternate ETW S3p FOS	6.92		7.16	0.55	7.96
Alternate UETW S3p FCS	7.31	1	7.31	0.55	7.47
Alternate UETW S3p FOS	7.35		7.35	1.73	23.49

TABLE III WINDING FACTOR OF WORKING HARMONIC

	All ETW S3p	All ETW D3p	Alternate ETW S3p	Alternate UETW S3p
$k_p = \begin{cases} \sin(p \frac{\pi}{N_s}), & \text{for ETW} \\ 1, & \text{for UETW} \end{cases}$	0.9659	0.9659	0.9659	1
$k_d = \frac{\sin(\frac{\pi}{m})}{N_s \sin(\frac{2\pi}{N_s})}$	0.9659	1	1	1
$k_w = k_p k_d$	0.9330	0.9659	0.9659	1

From Fig. 2 and TABLE II, some phenomena can be seen and explained:

(1) The average torque of the Alternate UETW S3p machine is the largest of all because of the highest winding factor for working harmonic no matter the machines adopt FCSs or FOSs. In contrast, the FCS Alternate ETW S3p machine has the lowest average torque among electrical machines with FCSs, which is different from the phenomenon seen in [3]-[9] where the Alternate ETW S3p machine with slot openings has larger average torque than the All ETW S3p machine. Although the Alternate ETW S3p machine has larger winding factor compared with the All ETW S3p machine, the local saturation caused by FCSs is severer in the former, which is the major reason for such phenomenon in FCS machines. For the specific electrical machines with FOSs here, the local saturation due to tooth-tip leakage does not exist [22]; therefore the variation of average torque coincides with the results reported before [3]-[9]. The All ETW D3p machine not only shows higher torque than All ETW S3p and Alternate ETW S3p machines but has lower torque ripple as well regardless of FCS/FOS machines.

(2) Referring to the parameter ‘Ratio’, it shows that the electrical machines with alternate teeth wound windings have higher saturation level than those having all teeth wound windings by adopting FCSs. In contrast, the magnetic circuit saturation levels are practically the same for ETW machines without tooth-tips, while the UETW machine without tooth-tips is less saturated because of the adjustment of stator yoke thickness. Both the local saturation introduced by FCSs and the influence of subharmonic from winding magnetomotive force (MMF) affect the magnetic circuit saturation. By the way, though the Alternate UETW S3p machine has lower saturation level than the Alternate ETW S3p machine, the UETW stator core structure reduces the slot area, which makes the winding accommodation more challenging.

(3) From the perspective of torque ripple, the adoption of FCSs will reduce the permeance variation from slotting effect, which leads to a lower fluctuation. The All ETW D3p machine shows the best performance for both FCS and FOS machines, while the Alternate UETW S3p machine has the highest fluctuation, especially for the machine with FOSs. Comparing the torque ripple of the All ETW S3p and Alternate ETW S3p machines, the latter one is larger and this is more obvious for FOS machines. The reason for torque ripple difference between these electrical machines is the different saturation level of magnetic circuit between each other. This can be seen from the stator core relative permeability distribution and the equal potential line distribution due to armature field only, as shown in Fig. 3 for FCS machines.

From Fig. 3, it can be seen that the influence of the 1st harmonic becomes increasingly high in the sequence of the All ETW D3p, All ETW S3p, Alternate ETW S3p and Alternate UETW S3p machines. The saturation of the stator yoke is accordingly affected, which leads to different output torque and torque ripple.

(4) There are 6 ripples over one electrical period for electrical machines adopting single 3-phase winding, whilst it is 12 for dual 3-phase winding. This will be explained from a more essential point of view, viz. the adjacent stator tooth

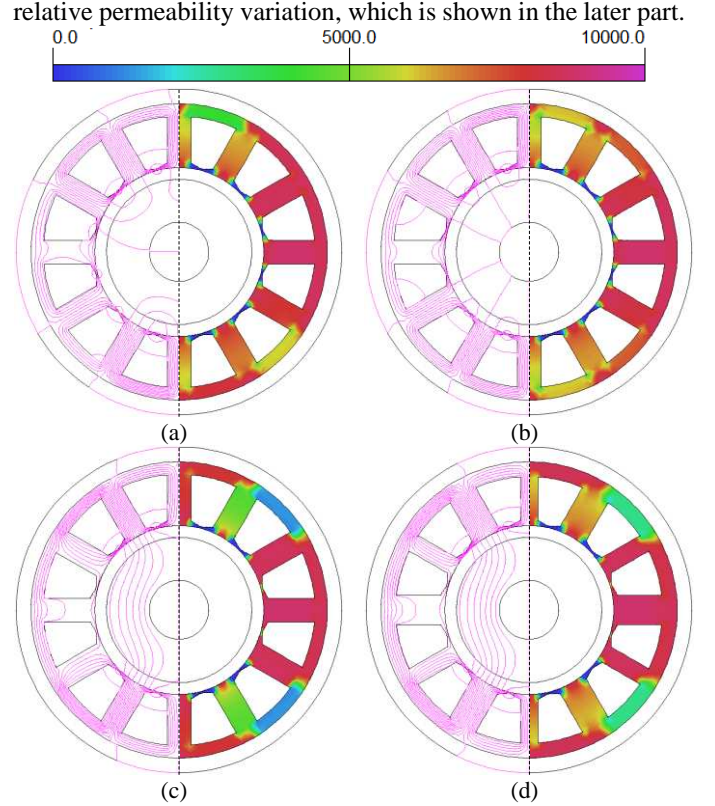


Fig. 3. Relative permeability distribution of stator and equal potential line distribution for armature field. (a) All ETW S3p. (b) All ETW D3p. (c) Alternate ETW S3p. (d) Alternate UETW S3p.

Overall, all of the electrical machines have their own specialties. The difference between them will be analyzed in detail in terms of torque performance. Since the electrical machines with slot openings have been reported in a large number of papers, this paper will focus on FCS ones.

B. Torque Component Separation

With the help of FP method (see Appendix), the on-load torque (OL) can be separated into three components, viz. PM component (PM), armature current component (Arm) and on-load cogging torque (Cog), respectively [18]. By analyzing each torque component, the characteristics of on-load torque can be clearly seen. The expressions of torque components under dq reference frame ($I_d=0$ control approach) are shown as follows:

$$T_{em} = T_{PM} + T_{arm} + T_{cog} \quad (3)$$

$$T_{PM} = \frac{3}{2} p [\psi_{dPM}(FP) I_q + \frac{d\psi_{qPM}(FP)}{d\theta_m} I_q] \quad (4)$$

$$T_{arm} = \frac{3}{2} p [\psi_{darm}(FP) I_q + \frac{d\psi_{qarm}(FP)}{d\theta_m} I_q] \quad (5)$$

$$T_{cog} = -\frac{\partial W_m(OL)}{\partial \theta_m} \quad (6)$$

where T_{em} is the on-load electromagnetic torque; T_{PM} , T_{arm} and T_{cog} are the PM, armature and cogging torque component,

respectively; $\psi_{dPM}(FP)$, $\psi_{qPM}(FP)$, $\psi_{darm}(FP)$ and $\psi_{qarm}(FP)$ are the on-load d- and q-axis PM and armature current flux-linkages predicted by FP method, respectively; p is the rotor pole pair number; I_q is the q-axis current and $W_m(OL)$ is the total stored magnetic energy under on-load condition. The process of employing frozen permeability method to separate on-load torque is briefly described in Appendix for clarity.

From eq. (3)-(6), it clearly shows that the on-load d- and q-axis flux-linkage (ψ_d and ψ_q) and the derivation of q-axis flux-linkage ($d\psi_q$) are crucial for torque prediction. Their waveforms are shown in Fig. 4.

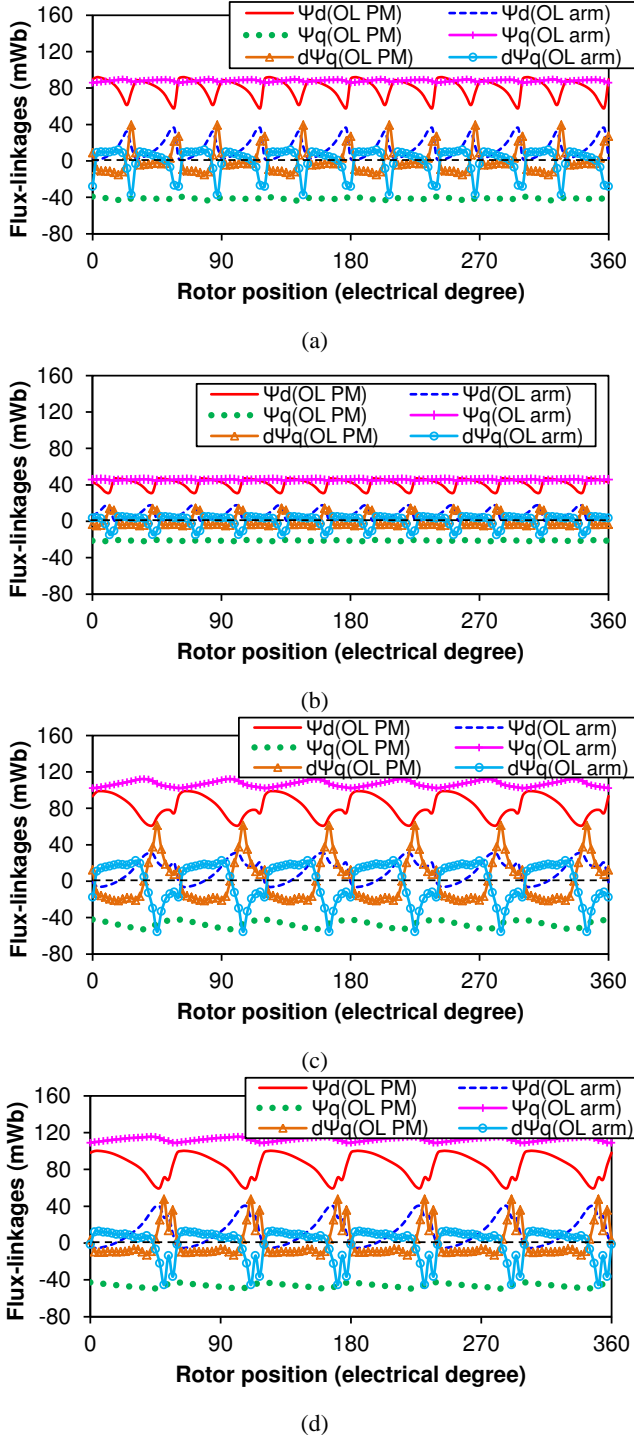
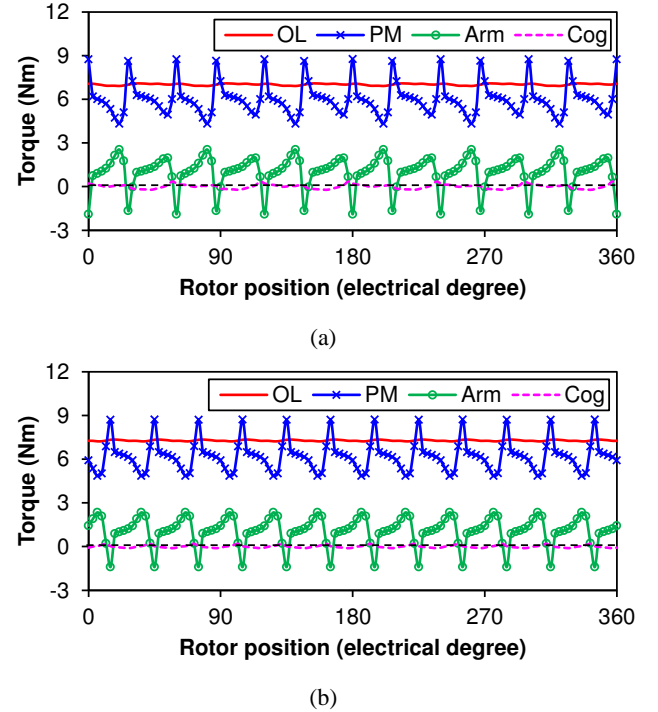
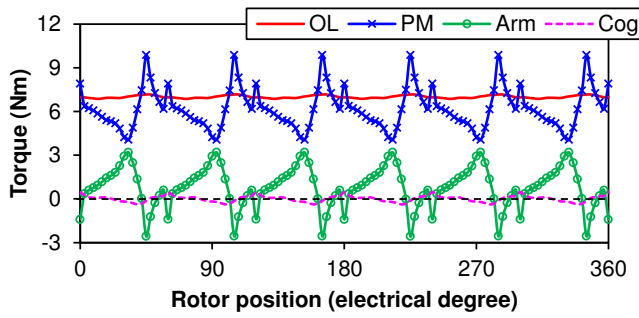


Fig. 4. Flux-linkages of four electrical machines. (a) All ETW S3p. (b) All ETW D3p. (c) Alternate ETW S3p. (d) Alternate UETW S3p.

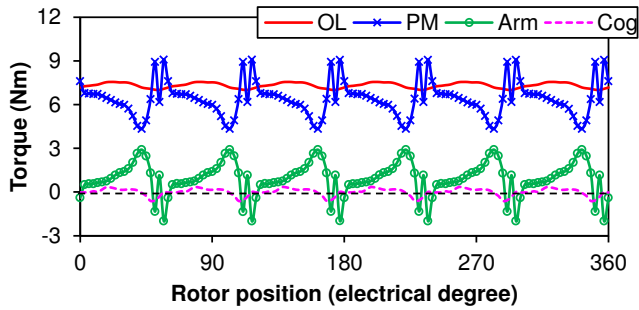
According to Fig. 4, all of the electrical machines have cross-coupling between d- and q-axis under on-load condition, since the q-axis PM and d-axis armature flux-linkage have non-zero average value. Ideally, both of them should be zero and the appearance of these components will affect the torque performance. The d-axis flux-linkage determines the average torque, while it also contributes to the torque ripple. For both PM and armature components of d-axis flux-linkage, the minimal fluctuation order is 6 for electrical machines with S3p windings. However, this lowest fluctuation number is 12 for the D3p machine, which is due to the merit of adopting dual 3-phase connection. The obvious fluctuation of both d-axis flux-linkage components is caused by the local saturation due to the FCS structure, which is closely related to the reason for voltage distortion shown in [22]. The difference of fluctuation amplitude reflects the influence of local saturation to some extent.

For q-axis flux-linkage, both PM and armature components have non-zero average value, whereas they will not contribute to average torque generation with $I_d=0$ control method. However, the derivation of q-axis flux linkage is one source of torque ripple according to eq. (3)-(6). The fluctuation period is the same as that of d-axis flux-linkage. The reason for more apparent spikes in the derivation of q-axis flux-linkage is the amplification effect of derivative operation. Based on the obtained flux-linkages and eq. (3)-(6), the waveforms of on-load torque and its three components are given in Fig. 5.





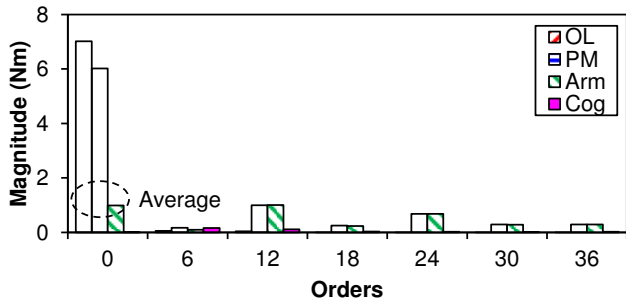
(c)



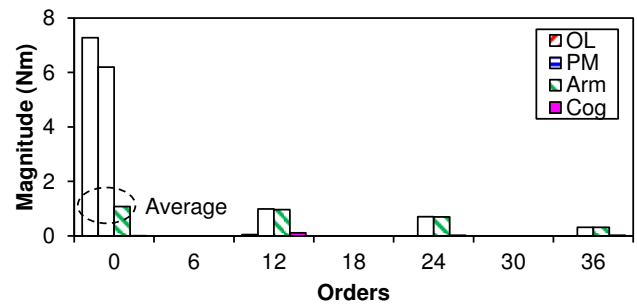
(d)

Fig. 5. Torque component waveforms of four electrical machines. (a) All ETW S3p. (b) All ETW D3p. (c) Alternate ETW S3p. (d) Alternate UETW S3p.

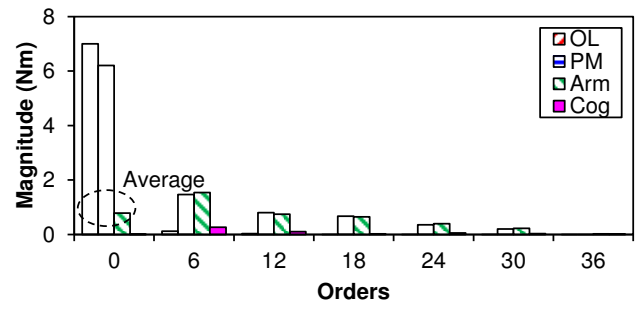
Fig. 5 shows that both PM and armature torque components obtained by using FP method have been apparently distorted due to the local saturation caused by FCS structure. However, these huge fluctuations will largely cancel each other out in the resultant on-load torque. The on-load cogging torque shown in Fig. 5 does not contribute to the average torque and it is only the source of torque ripple according to eq. (6). In fact, the cogging torque of these FCS machines is practically zero under open-circuit condition because of the smooth permeance variation, whereas they cannot be neglected under on-load situation due to the influence of armature reaction. In order to clearly see the contribution of each component to the on-load torque and make comparison among these electrical machines, the corresponding spectra are shown in Fig. 6.



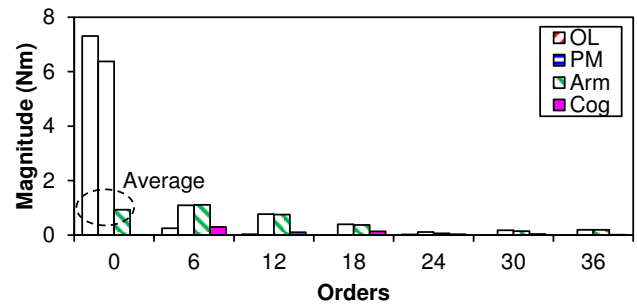
(a)



(b)



(c)



(d)

Fig. 6. Torque component spectra of four electrical machines. (a) All ETW S3p. (b) All ETW D3p. (c) Alternate ETW S3p. (d) Alternate UETW S3p.

The DC component in Fig. 6 is the average value. It clearly shows that the average value of on-load torque is the addition of PM and armature component, while the on-load cogging torque has no contribution. This coincides with eq. (3)-(6). For the high order harmonics, the magnitudes of PM and armature components are much higher than the corresponding on-load torque, which is owing to those obvious spikes shown in Fig. 5. Since the on-load cogging torque does not have these spikes, each higher order harmonic just has a bit larger magnitude compared with resultant on-load torque harmonics. The local saturation of tooth bridge area shown in Fig. 3 is the source for on-load cogging torque. When the rotor operates under on-load torque, the local saturation due to armature reaction will lead to the sharp variation of tooth bridge permeance, which has the equivalent effect of slotting. Thus, when the PM inter-region approaches the tooth bridge, the total stored energy will vary and on-load cogging torque is generated. The most important harmonic is 6, which is the major content of on-load torque ripple. The All ETW D3p machine does not have this

component due to the cancellation effect of dual 3-phase winding connection and the much lower 12th harmonic is the major source of torque ripple for this machine. The magnitude of the 6th harmonic increases in the sequence of the All ETW D3p, All ETW S3p, Alternate ETW S3p and Alternate UETW S3p machine. Therefore, the investigation of this harmonic is crucial to identify the difference of torque ripple for these machines.

C. The Reason for Torque Ripple Difference

As has been seen in the previous subsections, the difference of torque ripple for these machines is closely related to the machine saturation level which is affected by armature field. Thus, the air-gap flux density of these machines for armature field with rated current needs to be compared, as shown in Fig. 7.

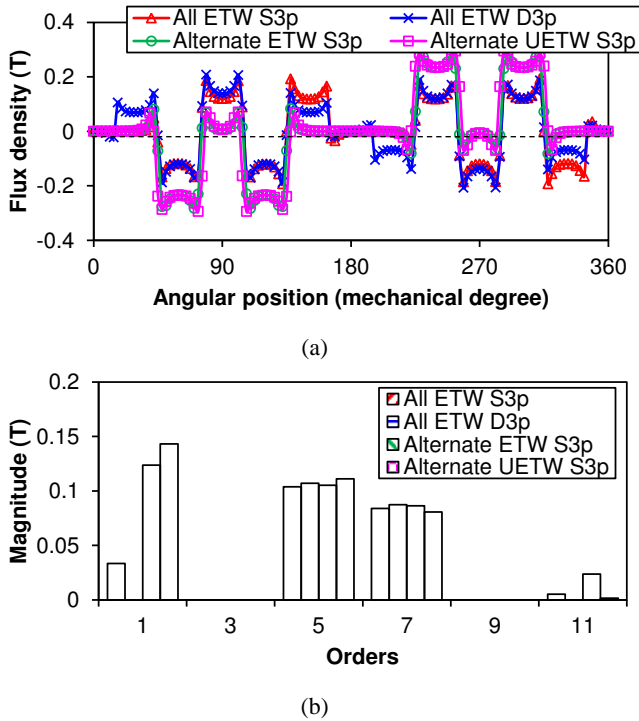
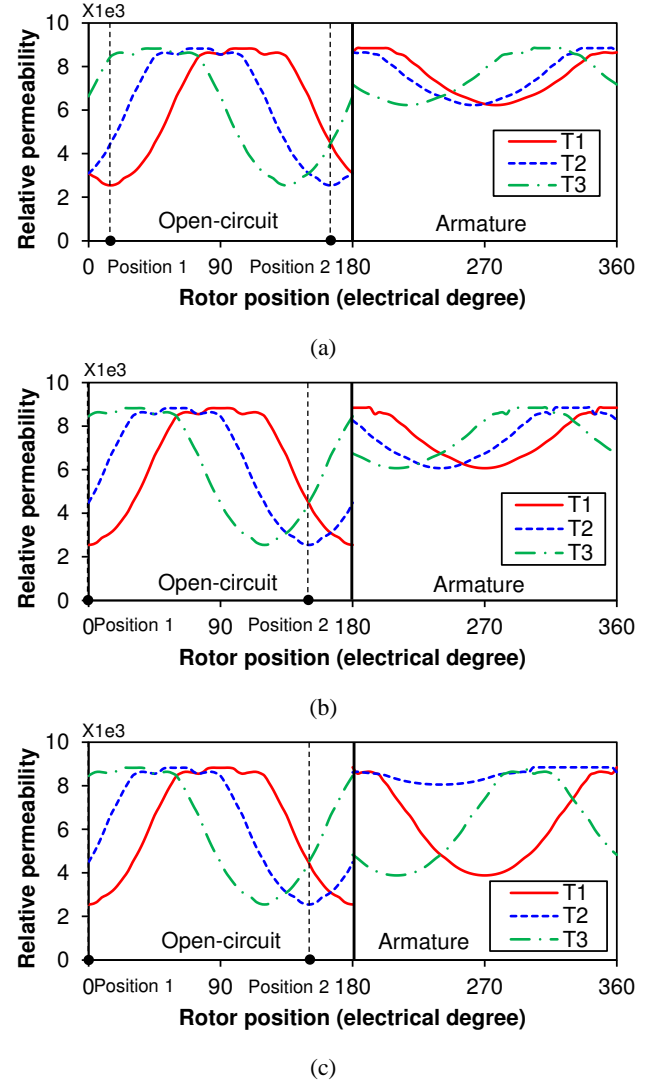


Fig. 7. Air-gap flux density due to armature field. (a) Waveforms. (b) Spectra.

Fig. 7(b) demonstrates that the 1st harmonic magnitude of air-gap flux density due to armature field varies in the same sequence as that of the 6th harmonic torque. The 5th harmonic in Fig. 7(b) is related to the average torque generation, while the 7th harmonic always exists, which is the intrinsic character of this electrical machine. The trend of the 5th harmonic magnitude is the same as that of average torque, which again shows the influence of local saturation caused by FCSs. For the Alternate UETW S3p machine, though the working harmonic increases, the harmful 1st harmonic component increases even higher. Thus, the most promising electrical machine is the All ETW D3p one. According to [4], the adoption of dual 3-phase winding configuration entirely eliminates the MMF harmonics with $t|12k\pm 1|$ ($k=0,1,2,\dots$) orders, where t is the greatest common divisor of slot and pole numbers. Furthermore, there is hardly saliency in SPM machines. Therefore, the 1st harmonic

does not exist in air-gap flux density due to armature field.

To show the influence of armature field and stator core structure on torque ripple, the relative permeability of adjacent stator teeth under open-circuit, armature and on-load conditions are all investigated. The teeth are grouped into two categories and the teeth within each group have the same saturation variation except the fixed phase shift between each other over one electrical period. The teeth having odd number belong to group 1, while the group 2 contains the teeth with even numbers, as shown in Fig. 1. The influence of the 1st harmonic on torque ripple difference will be reflected on these two groups and only tooth 1, 2 and 3 (T1, T2 and T3) are chosen for simplicity. The corresponding tooth relative permeability variation picked at the center of each tooth is shown in Fig. 8 for open-circuit and armature field.



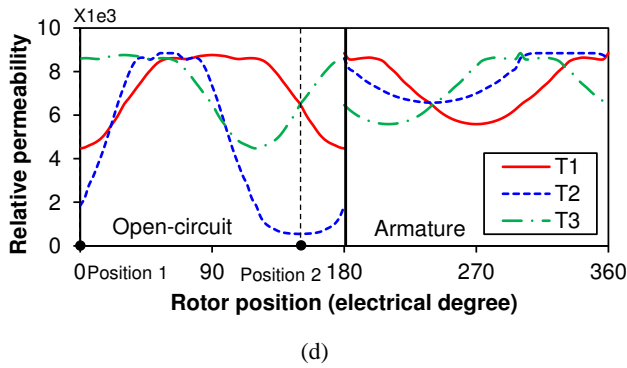


Fig. 8. Tooth relative permeability variation waveforms for PM and armature fields (12S/10P combination), respectively. (a) All ETW S3p. (b) All ETW D3p. (c) Alternate ETW S3p. (d) Alternate UETW S3p.

Fig. 8 shows that the open-circuit waveforms of teeth 1-3 are the same for ETW machines due to the same saturation level over one electrical period. However, the teeth in groups 1 and 2 are different for UETW machine due to the asymmetric stator core structure. For armature waveforms, only the All ETW D3p machine show the same waveforms for teeth 1-3, while other three machines have obvious difference between the teeth in groups 1 and 2. Since the tooth 2 shows quite different relative permeability variation, such difference between the teeth in groups 1 and 2 can be used to explain the torque ripple difference. When the effects of both open-circuit and armature act together, the resultant on-load relative permeability variation explains the reason for different average torque and torque ripple, as shown in Fig. 9.

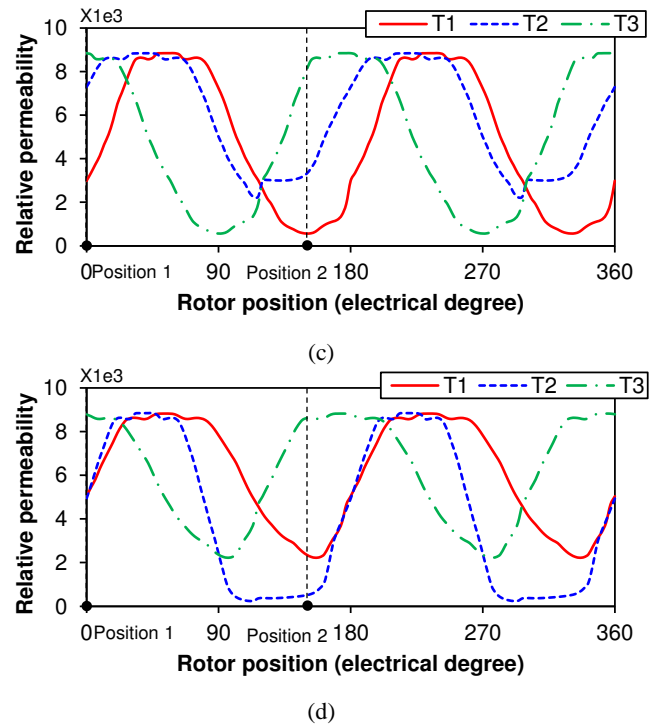
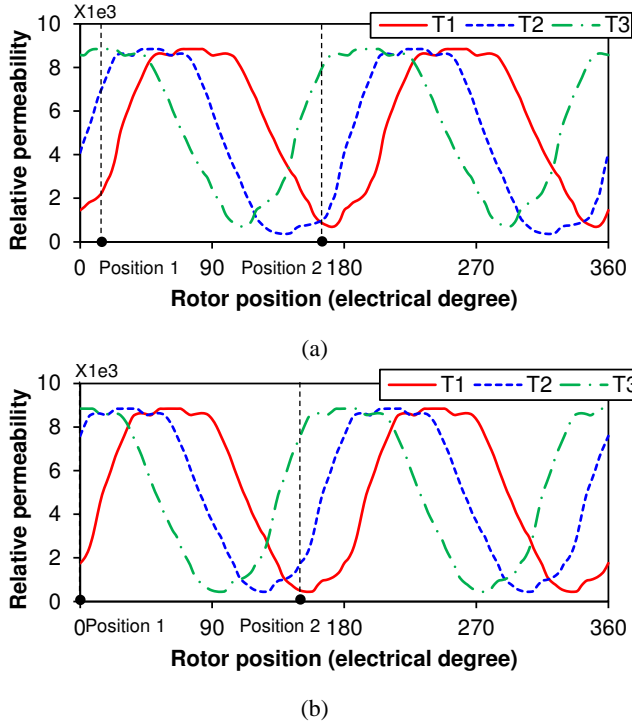


Fig. 9. Tooth relative permeability variation waveforms for on-load field (12S/10P combination), respectively. (a) All ETW S3p. (b) All ETW D3p. (c) Alternate ETW S3p. (d) Alternate UETW S3p.

Fig. 9 shows that the waveforms of teeth 1 and 3 are always the same no matter all or alternate teeth wound windings, ETW or UETW stator cores, S3p or D3p connections are used except with fixed 300 degree phase shift, which verifies the statement above. The difference between the teeth in groups 1 and 2 increases in the sequence of the All ETW D3p, All ETW S3p, Alternate ETW S3p and Alternate UETW S3p machines, which is the same as the torque ripple variation. Therefore, this kind of asymmetric saturation of adjacent stator teeth can be regarded as the major reason for torque ripple difference.

In order to further explain this adjacent stator teeth asymmetric saturation phenomenon, the virtual harmonic fields due to armature field at two specific positions are shown. Although the armature field contains abundant harmonics, only the three most important components, viz. 1, 5 and 7, are used to approximate. For the two specific positions, rotor d-axis coincides with the center of teeth 1 and 2, the magnetic circuit path for three representative harmonics are shown in Fig. 10. The solid, dotted and point lines are used to represent the 1st, 5th and 7th fields, respectively.

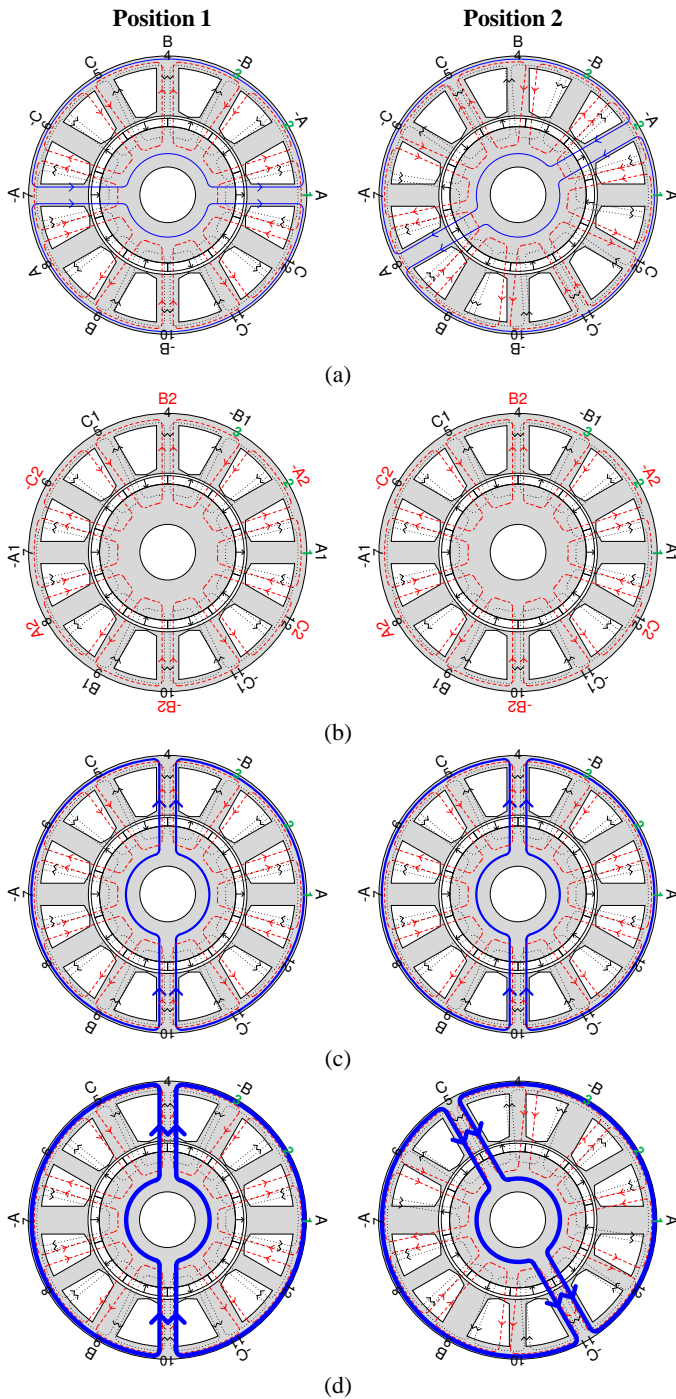


Fig. 10. Illustration of subharmonic influence. (a) All ETW S3p. (b) All ETW D3p. (c) Alternate ETW S3p. (d) Alternate UETW S3p.

When the 1st harmonic does not exist, there will not be difference between teeth 1 and 2, as shown in Fig. 10(b) for the All ETW D3p machine. This means that all of the teeth have the same saturation level over one electrical period and the torque ripple should be minimal compared with other electrical machines. With the increase of the 1st harmonic, the All ETW S3p machine shows some differences between teeth 1 and 2, as shown in Fig. 10(a). However, due to the small portion compared with the working harmonic, the influence is small and the torque ripple does not evidently increase. When the

alternate teeth wound winding is adopted, the amplitude of the 1st harmonic is beyond the working harmonic and its influence on torque ripple is obvious. Thus, the difference between teeth 1 and 2 is obvious for the Alternate ETW S3p machine, as shown in Fig. 10(c). For the Alternate UETW S3p one, the asymmetry due to UETW stator core structure will further aggravate such side effect, as shown in Fig. 10(d).

Overall, the higher level of adjacent stator teeth asymmetric saturation leads to the higher torque ripple. The subharmonic coming from winding topology and the stator asymmetric core structure like UETW are the two major factors.

D. Influence of current value

Since the armature field is affected by current value, the torque-current, PP torque-current and torque ripple-current characteristics are shown in Fig. 11 within three times of rated current.

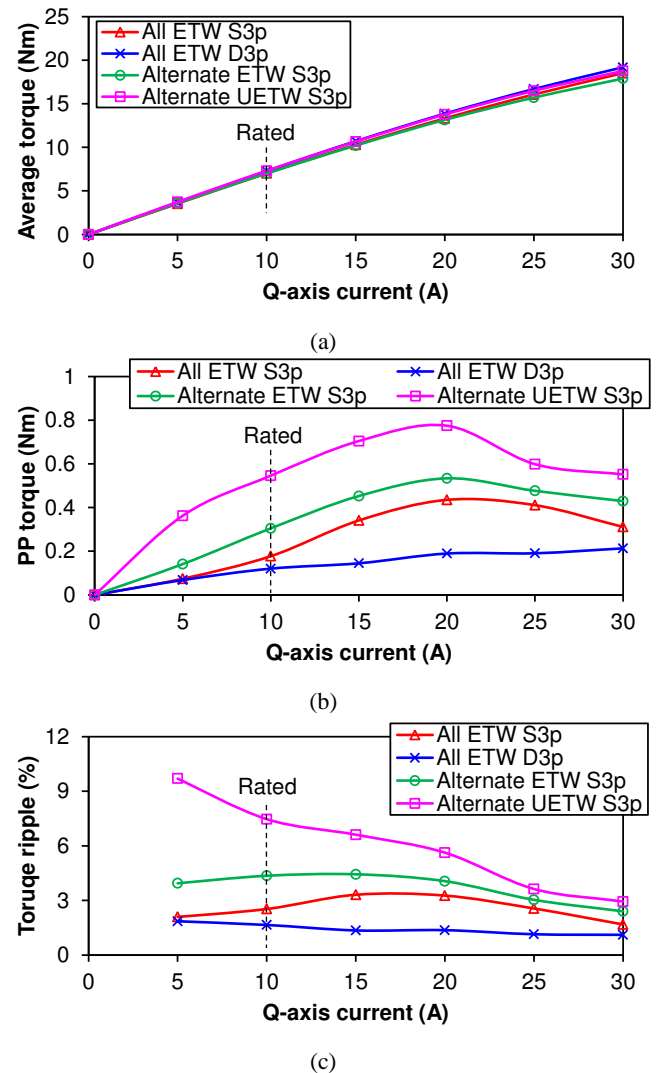


Fig. 11. Influence of current value on torque performances. (a) Torque-current characteristics. (b) PP torque-current characteristics. (c) Torque ripple-current characteristics.

It can be found that the saturation phenomenon appears for torque-current characteristic if the current is larger than rated value. When the current is three times of the rated value, the All

ETW D3p machine has the highest average torque among them. Due to the high saturation level, the average torque of the Alternate ETW S3p machine is the lowest. The saturation level of the Alternate UETW S3p machine is lower than the Alternate ETW S3p machine due to the increase of yoke thickness.

For PP torque-current characteristics, the All ETW D3p machine is still the best of all. As has been stated above, the 1st harmonic does not exist in this electrical machine and the torque ripple is minimal. The All ETW S3p machine is the 2nd best among them. Although the 1st harmonic exists in this electrical machine, its influence is decreased by phase winding distribution effect. With the increase of current, the PP torque of this machine has the peak value for a specific current. This probably comes from the phase variation of torque components with the increase of current. For this specific current, the resultant torque has the largest value. The Alternate ETW S3p and Alternate UETW S3p machines show the similar tendency. However, the torque ripple of these two machines is higher than all teeth wound machines. Besides, the Alternate ETW S3p machine has the lower torque ripple when the current is low and this will change with the increase of current.

When it comes to torque ripple-current characteristic, it can be seen as the combination of average torque and PP torque. With the increase of current, the saturation level has obvious change, which results in different torque ripple. The Alternate UETW S3p machine shows fast torque ripple reduction due to modification of stator yoke thickness to lower the stator saturation. For other three electrical machines, they show the similar phenomenon as shown in Fig. 11(b).

E. Influence of slot and pole number combinations

For the sake of further illustration, the complementary slot/pole number combination (12S/14P) is also analyzed. The same four prototype machines are compared and their cross-sections of FCS machines are shown in Fig. 12.

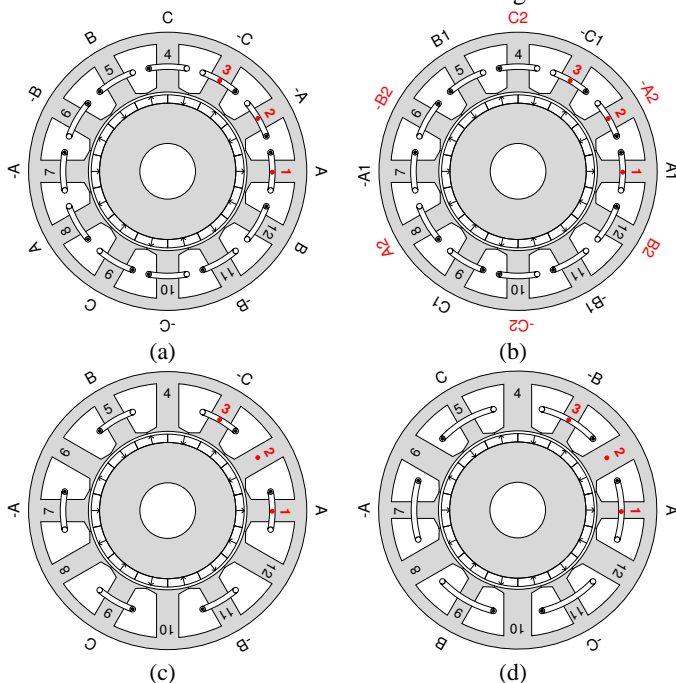


Fig. 12. Cross-sections of FCS machines with 12S/14P combination. (a) All ETW S. (b) All ETW D3p. (c) Alternate ETW S3p. (d) Alternate UETW S3p.

Comparing Fig. 12 and Fig.1, the major difference is the rotor pole number and the winding layout, while other structure parameters are kept the same for easy comparison. For all of the S3p machines, simply exchanging the phase B and C layouts of 12S/10P machines will lead to 12S/14P machine windings. If two sets of windings are changed in the same time, D3p for 12S/14P machine can be obtained as well. There is another obvious difference being observed for UETW machine. For the electrical machines with higher slot number than pole number, the coils will be wound on thicker teeth to capture more effective flux, while it is the thinner teeth that should be wound if the slot number is smaller than pole number [24]. When the same rated current is fed into windings, the torque performance is shown in Fig. 13.

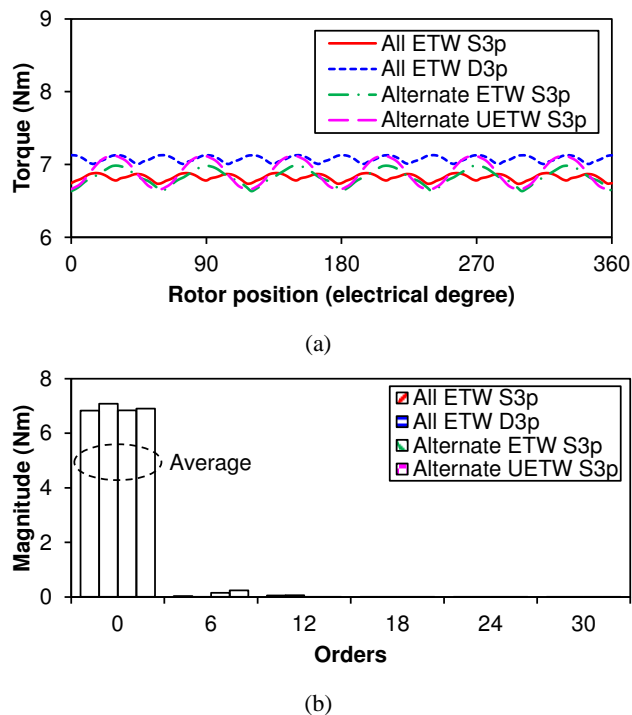
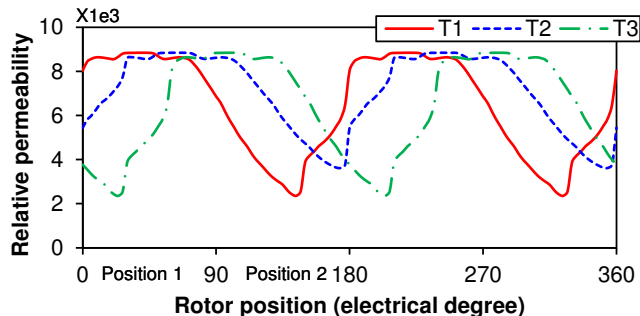


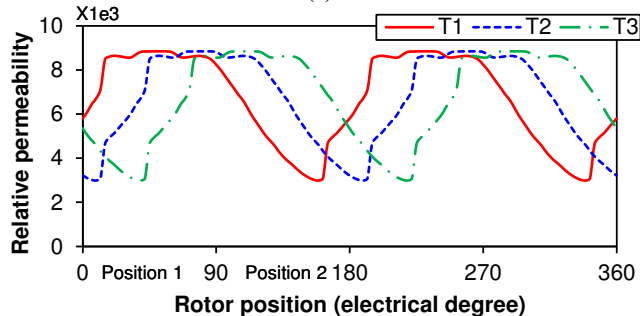
Fig. 13. On-load torque comparison for FCS 12S/14P machines (Rated). (a) Waveforms. (b) Spectra.

The waveforms in Fig. 13(a) show that the electrical machines with 12S/14P combination will have smoother instant torque compared with the counterpart electrical machines with 12S/10P combinations. Besides, the average torque and torque ripple will also be different. Fig. 13(b) can more clearly explain the difference. For DC component, the All EYW D3p machine has the largest value, while the Alternate UETW S3p machine has a bit lower value. This is different from the results shown in Fig. 2. The winding layout difference of 12S/10P and 12S/14P UETW machines is the reason. For 12S/14P machine, the thinner teeth is much easier to be saturated by armature field; therefore its average torque improvement effect will not be as strong as the adoption of D3p winding. However, the larger winding factor still guarantees larger value than All ETW S3p

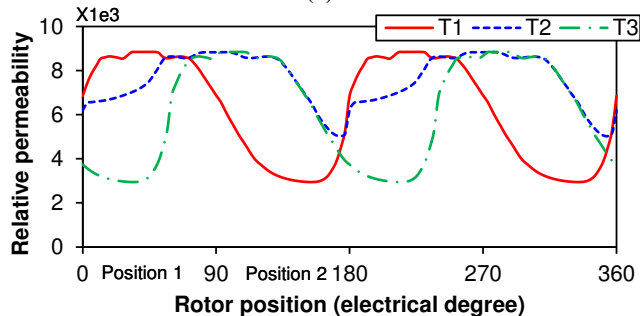
and Alternate ETW S3p machines. The influence of local saturation again makes the merit of using alternate teeth wound negligible. When it comes to the torque ripple, the value still decreases in the sequence of Alternate UETW S3p, Alternate ETW S3p, All ETW S3p and All ETW D3p machines. This coincides with the conclusion drawn before. The asymmetric saturation level of adjacent teeth is closely related with the torque ripple. Similar to Fig. 9, the on-load relative permeability of three teeth is shown in Fig. 14 to verify the statement.



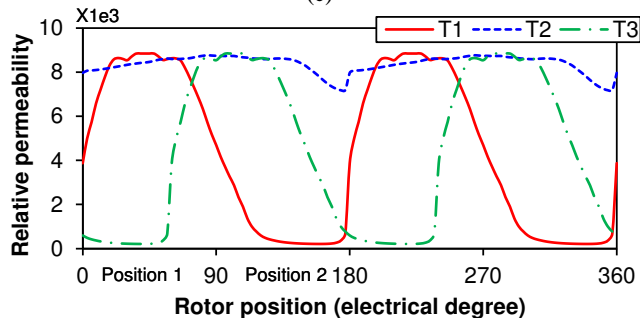
(a)



(b)



(c)



(d)

Fig. 14. Tooth relative permeability variation waveforms for on-load field (12S/14P combination), respectively. (a) All ETW S3p. (b) All ETW D3p. (c) Alternate ETW S3p. (d) Alternate UETW S3p.

Fig. 14 demonstrates that the level of saturation difference of adjacent teeth is consistent with the torque ripple. When adjacent teeth have larger difference in terms of relative permeability, the torque ripple will be larger. The UETW stator core and S3p winding result in the largest asymmetric saturation for adjacent teeth, which leads to the largest torque ripple. In contrast, the ETW and D3p winding makes each tooth saturation level the same. Thus, the torque ripple is the lowest for the All ETW D3p machine. For other two electrical machines, the heavier asymmetric saturation of adjacent teeth can be seen for of the Alternate ETW S3p machine. That is to say, the larger torque ripple will be generated.

It can be seen that the conclusion drawn based on 12S/10P machine analysis can be employed to complementary 12S/14P combination. Therefore, the conclusion should be also valid for electrical machines with other slot/pole number combinations.

IV. EXPERIMENTAL VALIDATION

For the FCS PM machines analyzed in this paper, two prototypes have been built. They are the All ETW S3p and Alternate ETW S3p machines, as shown in Fig. 15.

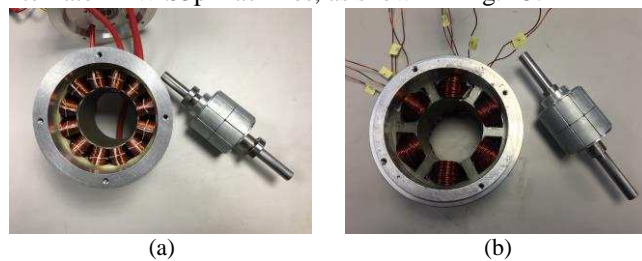


Fig. 15. Prototype machines with 12S/10P combination. (a) All ETW S3p. (b) Alternate ETW S3p.

The open-circuit back-EMF waveforms of two electrical machines are measured, as shown in Fig. 16. It can be seen that the measured back-EMFs are a bit lower than the 2D finite element (FE) predicted one due to the end-effect and practically the same as the 3D FE result. There are still some slight differences, since the 3D FE modelling of the end region is pretty hard and the measurement errors are unavoidable in reality. Besides, the Alternate ETW S3p machine has a larger open-circuit back-EMF than the All ETW S3p machine for both predicted and measured results since the winding factor for the Alternate ETW S3p machine is larger. This is consistent with the phenomena reported in existing papers [4]-[7].

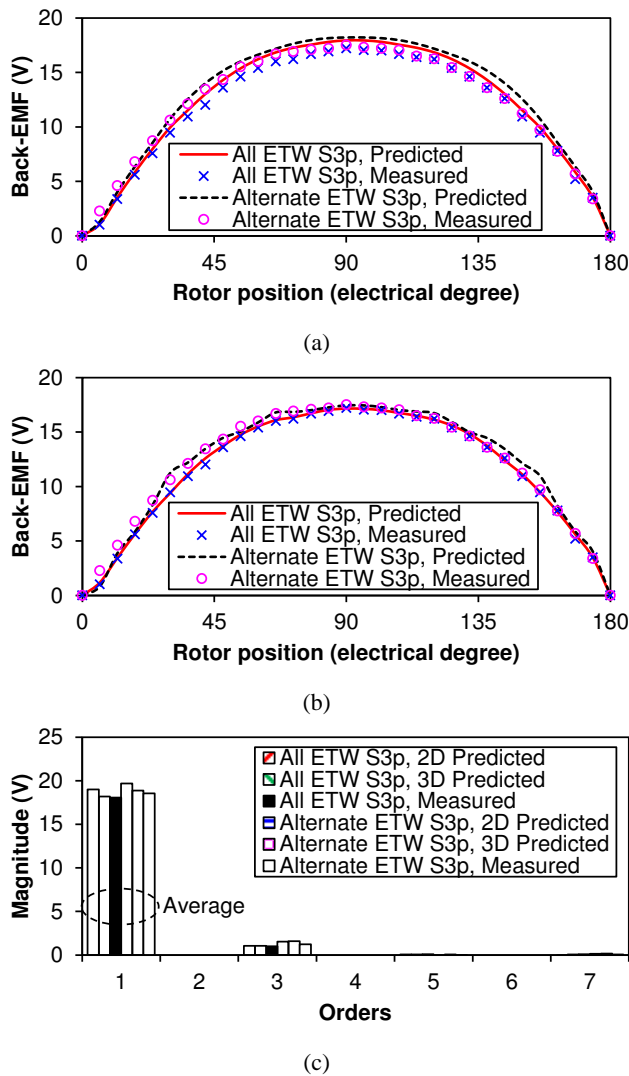


Fig. 16. Comparison of predicted and measured open-circuit back-EMFs under 400 rpm. (a) Waveforms for 2D. (b) Waveforms for 3D (c) Spectra.

For these two electrical machines, the measured torque variations with the rotor position over one electrical period are shown in Fig. 17, together with the 2D and 3D FE results. The torque-current characteristics are also measured and compared with the predicted ones, as shown in Fig. 18. It shows that overall the predicted and measured results match well, although both the average torque and torque ripple are a bit different between 2D FE and measure results. The end effect leads to the reduction of average torque, while the torque ripple difference is caused by measurement error. However, 3D FE results match the measurement better except some small discrepancies, since the on-load torque ripple is very hard to measure. Moreover, in contrast to the open-circuit back-EMF, the Alternate ETW S3p machine has lower average torque and higher torque ripple than the All ETW S3p counterpart due to more heavily saturated stator under on-load condition. With the increase of current, the difference between two machines will be larger. Since the current for measurement cannot exceed the rated one for the prototypes, the zoom is used to show the phenomenon in Fig.

18. This further explains the influence of stator core saturation. Thus, both the FE analyses and experimental results have verified that the analyses in the paper. Furthermore, the comparison of torque-current characteristics over rated current value can be seen in Fig. 11.

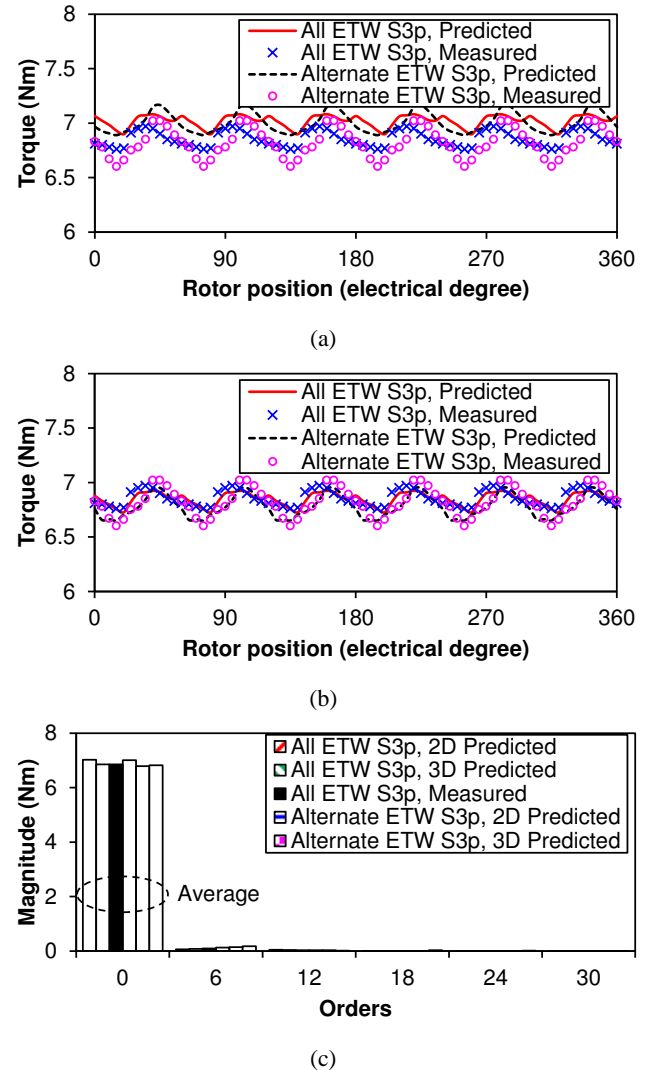


Fig. 17. Comparison of predicted and measured torque with rated current. (a) Waveforms for 2D. (b) Waveforms for 3D (c) Spectra.

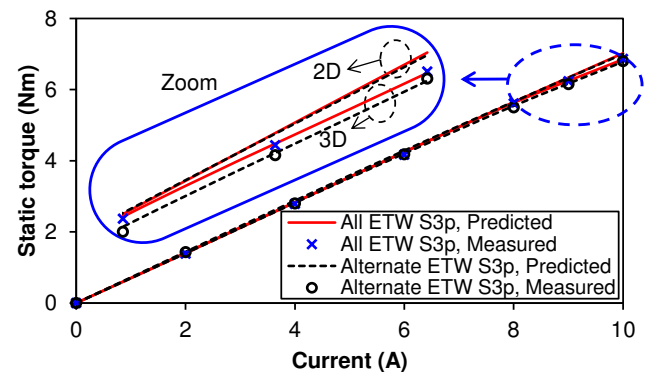


Fig. 18. Comparison of predicted and measured torque-current characteristics within rated current range.

V. CONCLUSION

From the torque comparison of 12S/10P fractional-slot SPM machines with FCSs and different stator topologies, it can be found that the alternate teeth wound machines have larger torque ripple compared to all teeth wound machines having the same dimensions. This is mainly due to the adjacent stator teeth asymmetric saturation caused by the armature reaction. The dual 3-phase winding shows the best torque performance among them due to its elimination of the subharmonic and having the lowest local saturation due to FCSs. Furthermore, the UETW stator used to improve the output torque can lead to the highest torque ripple under rated operation condition, since it further aggravates the asymmetry of stator saturation. Although current value will affect the torque performances, the major conclusion is practically the same. Therefore, the selection of machines is a compromise between average torque and torque ripple except adopting a complicated dual 3-phase winding. Two prototype machines have been built, and the predictions have been validated by measurements. Although 12S/10P machines with FCSs have been investigated in this paper, the similar conclusion can also be applicable to FOS machines except some minor changes due to the influence of slot opening. Besides, the same conclusions can be obtained for other fractional-slot SPM machines with different slot/pole number combinations, as analyzed on complementary 12S/14P combination.

APPENDIX

The principle of FP method can be explained based on Fig. 19.

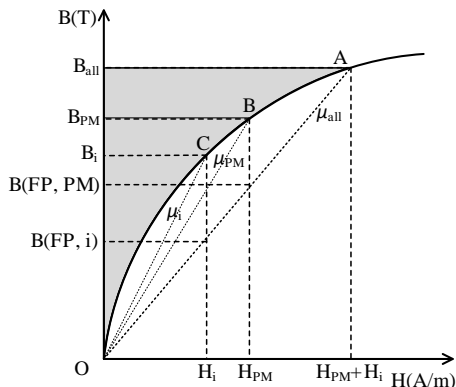


Fig. 19. Illustration of FP method.

For the nonlinear B-H curve of lamination shown in Fig. 19, the open-circuit flux density is B_{PM} , which is excited due to PM field intensity- H_{PM} . The relative permeability will be μ_{PM} under such condition. If only armature currents exist, the field intensity- H_i will generate its corresponding flux density- B_i as well. Under such situation, the relative permeability will be μ_i . It is clear that the relative permeability of two cases will be different. When both sources exist, the resultant field intensity ($H_{PM}+H_i$) will produce the on-load flux density- B_{all} . Although the on-load field intensity can be simply added by PM and armature field intensity, B_{all} does not satisfy this relationship with B_{PM} and B_i due to the material nonlinear property. In order to solve this problem, the on-load field is predicted by finite element analysis (FEA) firstly. Then the relative permeability of each mesh element (μ_{all}) is frozen for the following analysis. After this, the

nonlinear magnetic circuit is degraded into linear type and the influence of PM and armature fields can be separated.

The process of employment this method to obtain PM and armature components of on-load torque is summarized in Fig. 20.

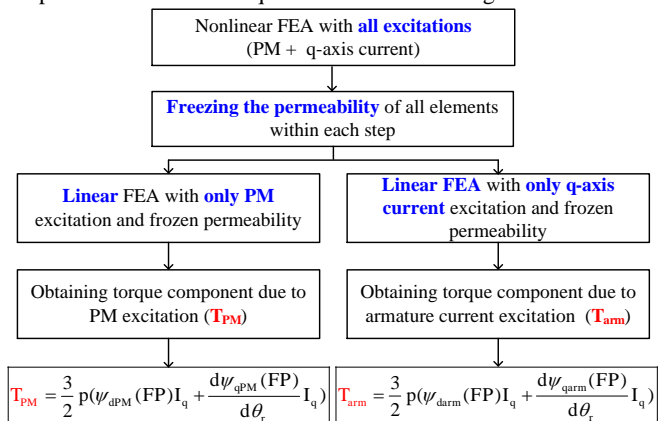


Fig. 20. Employment of FP method to predict PM and armature torque components.

According to (3) and (6), the on-load torque not only contains PM and armature components, but also has another term which accounts for the variation of total stored energy under on-load condition. This term is defined as on-load cogging torque. Different from the conventional open-circuit cogging torque, the on-load cogging torque considers the influence of armature field on saturation. Fig. 19 is used to explain the difference between open-circuit and on-load stored energies in nonlinear part of electrical machines. The area filled with slash lines represents the open-circuit stored energy, while the whole shaded area is the total stored energy under on-load condition. The derivation of these two different quantities leads to open-circuit and on-load cogging torque, respectively. It is clear that the on-load cogging torque accounts both PM and armature field influence together. The process of predicting this quantity is given in Fig. 21.

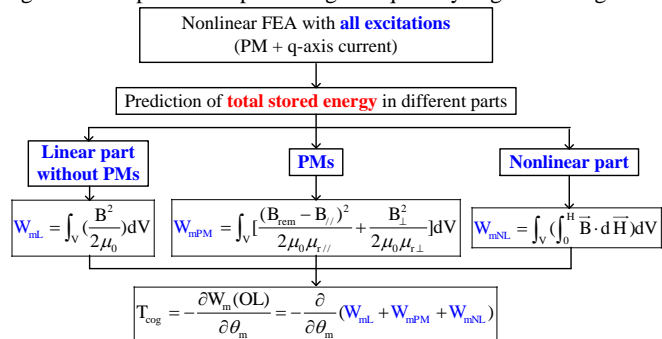


Fig. 21. On-load cogging torque prediction process.

Fig. 21 shows that $W_m(OL)$ consists of three parts, viz. linear part without PMs (W_{ml}), PMs (W_{mPM}) and nonlinear part (W_{mNL}), respectively. The stored energy of each part can be obtained by the integral of the energy density over the corresponding volume. For linear part without PMs, the flux density (B) and air permeability can be used to represent energy density. Since PMs have remanence (B_{rem}), the PM flux density must be considered in orthogonal magnetization parallel and vertical directions ($B_{//}$ and B_{\perp} , respectively). The relative permeability in two directions ($\mu_{r//}$ and $\mu_{r\perp}$ for magnetization parallel and vertical directions, respectively) should be separately considered as well. The most complicated portion is the nonlinear part, where the integral of nonlinear B-H curve is needed. After obtaining the stored energy of three parts, the total stored energy is synthesized and the

on-load cogging torque can be obtained.

REFERENCES

- [1] A. M. El-Refaie, "Fractional-slot concentrated-windings synchronous permanent magnet machines: opportunities and challenges," *IEEE Trans. Ind. Electron.*, vol. 57, no. 1, pp. 107-121, Jan. 2010.
- [2] J. Cros, and P. Viarouge, "Synthesis of high performance PM motors with concentrated windings," *IEEE Trans. Energy Convers.*, vol. 17, no. 2, pp. 248-253, June 2002.
- [3] N. Bianchi, and M. D. Prè, "Use of the star of teeth in designing fractional-slot single-layer synchronous motors," *IEE Proc.-Electr. Power Appl.*, vol. 153, no. 3, pp. 459-466, May 2006.
- [4] N. Bianchi, M. D. Prè, G. Grezzani, and S. Bolognani, "Design considerations on fractional-slot fault-tolerant synchronous motors," *IEEE Trans. Ind. Appl.*, vol. 42, no. 4, pp. 997-1006, July/Aug. 2006.
- [5] M. Popescu, D. G. Dorrell, D. Ionel, and C. Cossar, "Single and double layer windings in fractional slot-per-pole PM machines - effects on motor performance," in *34th Annual Conference of IEEE Industrial Electronics (IECON 2008)*, 10-13 Nov., 2008, pp. 2055-2060.
- [6] F. Magnussen, and H. Lendenmann, "Parasitic effects in PM machines with concentrated windings," *IEEE Trans. Ind. Appl.*, vol. 43, no. 5, pp. 1223-1232, Sept./Oct. 2007.
- [7] A. M. El-Refaie, and T. M. Jahns, "Optimal flux weakening in surface PM machines using fractional-slot concentrated windings," *IEEE Trans. Ind. Appl.*, vol. 41, no. 3, pp. 790-800, May/June 2005.
- [8] J. B. Wang, K. Atallah, Z. Q. Zhu, and D. Howe, "Modular three-phase permanent-magnet brushless machines for in-wheel applications," *IEEE Trans. Veh. Technol.*, vol. 57, no. 5, pp. 2714-2720, Sept. 2008.
- [9] P. B. Reddy, A. M. El-Refaie, and H. Kum-Kang, "Effect of number of layers on performance of fractional-slot concentrated-windings interior permanent magnet machines," *IEEE Trans. Power Electron.*, vol. 30, no. 4, pp. 2205-2218, Apr. 2015.
- [10] M. Barcaro, N. Bianchi, and F. Magnussen, "Configurations of fractional-slot IPM motors with dual three-phase winding," in *IEEE International Electric Machines and Drives Conference (IEMDC 2009)*, May 3-6, 2009, pp. 936-942.
- [11] M. Barcaro, N. Bianchi, and F. Magnussen, "Analysis and tests of a dual three-phase 12.slot 10.pole permanent-magnet motor," *IEEE Trans. Ind. Appl.*, vol. 46, no. 6, pp. 2355-2362, Nov./Dec. 2010.
- [12] D. Ishak, Z. Q. Zhu, and D. Howe, "Permanent-magnet brushless machines with unequal tooth widths and similar slot and pole numbers," *IEEE Trans. Ind. Appl.*, vol. 41, no. 2, pp. 584-590, Mar./Apr. 2005.
- [13] S. P. Cheng, and C. C. Hwang, "Design of high-performance spindle motors with single-layer concentrated windings and unequal tooth widths," *IEEE Trans. Magn.*, vol. 43, no. 2, pp. 802-804, Feb. 2007.
- [14] P. Ponomarev, I. Petrov, and J. Pyrhonen, "Torque ripple reduction in double-layer 18/16 TC-PMSMs by adjusting teeth widths to minimize local saturation," in *21th International Conference on Electrical Machines (ICEM 2014)*, 2-5 Sept., 2014, pp. 1461-1467.
- [15] I. Petrov, P. Ponomarev, Y. Alexandrova, and J. Pyrhonen, "Unequal teeth widths for torque ripple reduction in permanent magnet synchronous machines with fractional-slot non-overlapping windings," *IEEE Trans. Magn.*, vol. 51, no. 2, pp. 1-9, Feb. 2015.
- [16] M. Barcaro, N. Bianchi, and F. Magnussen, "Remarks on torque estimation accuracy in fractional-slot permanent-magnet motors," *IEEE Trans. Ind. Electron.*, vol. 59, no. 6, pp. 2565-2572, June 2012.
- [17] W. Q. Chu, and Z. Q. Zhu, "Average torque separation in permanent magnet synchronous machines using frozen permeability," *IEEE Trans. Magn.*, vol. 49, no.3, pp. 1202-1210, Mar. 2013.
- [18] D. Wu, and Z. Zhu, "Design trade-off between cogging torque and torque ripple in fractional slot surface-mounted permanent magnet machines," *IEEE Trans. Magn.*, vol. 15, no. 11, pp. 1-4, Nov. 2015.
- [19] A. Roekke, and R. Nilssen, "Analytical calculation of yoke flux patterns in fractional-slot permanent magnet machines," *IEEE Trans. Magn.*, vol. 53, no. 4, pp. 1-9, Apr. 2017.
- [20] N. Bianchi, and S. Bolognani, "Design techniques for reducing the cogging torque in surface-mounted PM motors," *IEEE Trans. Ind. Appl.*, vol. 38, no. 5, pp. 1259-1265, Sept./Oct. 2002.
- [21] H. V. Xuan, D. Lahaye, H. Polinder, and J. A. Ferreira, "Influence of stator slotting on the performance of permanent-magnet machines with concentrated windings," *IEEE Trans. Magn.*, vol. 49, no. 2, pp. 929-938, Feb. 2013.
- [22] D. Wu, and Z. Zhu, "On-load voltage distortion in fractional slot surface-mounted permanent magnet machines considering local magnetic saturation," *IEEE Trans. Magn.*, vol. 51, no. 8, pp. 1-10, Aug. 2015.
- [23] Y. X. Li, Z. Q. Zhu, and G. J. Li, "Torque investigation of fractional-slot permanent magnet machines with different winding topology and stator structures," in *8th International Conference on Ecological Vehicles and Renewable Energies (EVER 2016)*, Apr. 4-8, 2016, pp. 1-8.
- [24] G. J. Li, Z. Q. Zhu, M. P. Foster, and D. A. Stone, "Comparative studies of modular and unequal tooth PM machines either with or without tooth tips," *IEEE Trans. Magn.*, vol. 50, no. 7, pp. 1-10, July 2014.